

Energy Transfer Efficiency based on One- and Two-Photon FRET Microscopy Differentiates Between Clustered and Random Distribution of Membrane-bound Receptor-ligand Complexes

Horst Wallrabe^a, Masilamani Elangovan^b, Almut Burchard^c and Margarida Barroso^{a1}

^aUniversity of Virginia, Dep. of Biology, Gilmer Hall, 057, Charlottesville, VA 22904

^bW. M. Keck Center for Cellular Imaging, University of Virginia, Dep. of Biology, Gilmer Hall, 064, Charlottesville, VA 22904

^cUniversity of Virginia, Dep. of Mathematics, Kerchof Hall, 303, Cabell Drive, Charlottesville, VA 22904

ABSTRACT

We are investigating membrane-based sorting processes in polarized epithelial MDCK cells, which most likely involves membrane microdomains. We have postulated that proteins contained in these microdomains, cluster, and to prove this, we have internalized differently fluorophore labeled pIgA-R ligands in MDCK cells, stably transfected with polymeric IgA receptors (pIgA-R), from opposite plasma membranes. Our previous work showed that these receptor-ligand complexes colocalize in the apical recycling endosome (ARE), underneath the apical plasma membrane. Quantitative one-photon confocal and 2-photon (2-P) FRET microscopy allowed us to calculate energy transfer efficiency (E%). Unquenched donor levels were established based on a novel algorithm, which corrects the FRET contamination of acceptor bleed-through and donor crosstalk. Using different emission filters also confirmed the veracity of the algorithm. 2-P FRET allows the selection of a specific donor wavelength, which does not precipitate acceptor bleed-through, a clear advantage over 1-P confocal microscopy. Results show that E% is independent of acceptor levels, an indication of a clustered distribution, as in random distribution E% rises with increasing acceptor levels. However, E% decreases with increasing donor and donor:acceptor ratio levels, which we have termed donor geometric exclusion, where some donors in a cluster block others from interacting with an acceptor. We submit that this is a second indicator for a clustered pattern, because in a random, dispersed situation donors are not likely to be in close proximity to have such an effect. We have developed a model explaining this phenomenon.

Keywords: MDCK cells, pIgA-R, apical recycling endosome (ARE), one-photon(1-P) FRET microscopy, two-photon (2-P) FRET microscopy, energy transfer efficiency (E%), contamination correction algorithm, clustered distribution, microdomains.

1. INTRODUCTION

Differentiating between clustered and random distribution of cellular components (proteins, lipids etc.) and estimating the distance between these components can be achieved with fluorescence resonance energy transfer (FRET) microscopy, using either conventional one-photon (1-P) confocal or two-photon (2-P) fluorescence imaging microscopy¹⁻³. The basis for such calculations is the FRET energy transfer efficiency (E%), which in turn can only be used with confidence, after the FRET signal has been corrected for the fluorescence spillover contamination. This contamination occurs as a result of the spectral overlap between donor and acceptor (Fig.1), which is necessary for FRET to occur in the first place. Other conditions for FRET to occur are that donor and acceptor have to be within a distance of 10-100 Å and also have a favorable dipole-dipole orientation between the two molecules. There are two major contaminants that spill over into the FRET channel along with the actual FRET signal: the overlap of the donor emission spectrum with that of the acceptor ('donor crosstalk') and that part of the acceptor absorption spectrum that is affected by the donor excitation wavelength ('acceptor bleed-through') (Fig.1). Different correction methodologies exist⁴⁻⁸; here we have developed a highly sensitive algorithm based on single label reference specimens, which corrects

¹ Correspondence: E-mail: mmb8n@virginia.edu; Telephone: 434-243-7616; Fax 434-982-5626

the contaminated FRET signal pixel-by-pixel⁹. To verify the robustness of the algorithm, we have compared fluorescence data acquired with different emission filters, capturing different levels of FRET signals with their associated different spillover contamination and found comparable energy efficiency transfer (E%) values using 1-P and 2-P microscopy.

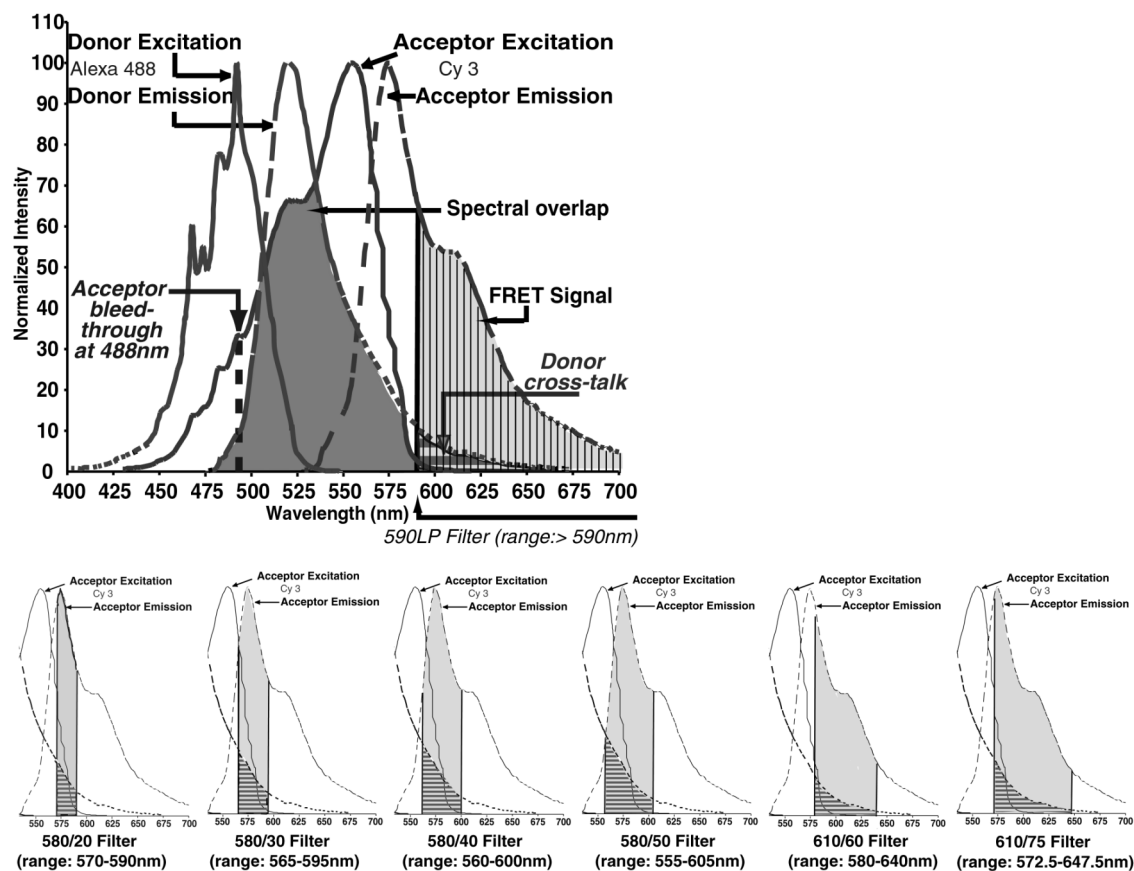


Figure 1. The FRET signal contains two contaminants (donor crosstalk and acceptor bleed-through), which can be reduced by different emission filters at the cost, however, of the level of FRET signal. This problem becomes less critical with our novel algorithm.

We have used and improved an assay which uses the relationship of E% to donor, acceptor and donor : acceptor (D:A) ratios to determine whether the distribution of protein complexes in our experiments is random or clustered¹⁰. For our experiments, we have used polarized epithelial MDCK cells which have two distinct plasma membranes (apical and basolateral), allowing us to internalize pIgA-R-ligands conjugated to two different fluorophores: Alexa 488 acting as the donor and Cy 3 acting as the acceptor. Our previous work has shown that these receptor-ligand complexes colocalize in the apical recycling endosome (ARE)¹¹, underneath the apical PM. In our current work we are able to quantify such colocalization to the level of fully resolved pixels of 88 nm x 88 nm and our results confirm a clustered distribution of pIgA-receptor-ligand complexes in the ARE of polarized epithelial MDCK cells, probably representing part of a membrane microdomain formation and sorting mechanism. We have also developed a clustered distribution model, which explains the phenomenon of 'donor geometric exclusion', which we regard as an additional determinant of a clustered distribution pattern.

2. METHODOLOGIES

2.1 Growing MDCK Cells on Filter Inserts

MDCK cells stably transfected with pIgA-R were grown to confluence in 100mm cell culture dishes. After four days, the cells were trypsinized, centrifuged and resuspended in DMEM/10% FBS/Pen-Strep¹¹. 120 μ l of the cell suspension were placed on top of an inverted Transwell Clear insert (Corning Costar, Cambridge, MA), i.e. on the outside of the membrane. To prevent the cell suspension from spilling over the edge of the insert, a temporary parafilm collar was placed around the inset under sterile conditions¹². Growing cells on the outside of the insert allows the visualization of the MDCK cells directly through a coverslip using an inverted microscope. After the cells attach to the membrane in approximately four hours, the parafilm collar is removed and the inserts are placed the normal way into multi-well dishes containing DMEM/10%FBS/Pen-Strep. After 3 days in culture these cells are fully polarized and are used immediately according to specific internalization protocols¹¹.

2.2 Internalizing Fluorophore-Labeled Ligands

The inserts with polarized MDCK cells are washed with PBS and equilibrated with DMEM/HEPES/BSA at 17 $^{\circ}$ C. 160 μ g/ml pIgA-R-IgG ligands ([Fab]₂ pseudo ligands) conjugated to Alexa488 (Molecular Probes, Eugene, OR) or Cy3 (Amersham Life Science, Pittsburgh, PA) are applied to the apical and basolateral PM, respectively. Cells are incubated at 17 $^{\circ}$ C for four hours to allow internalization of pIgA-R-ligand complexes into the sub-apical region by transcytosis from the basolateral towards the apical PM and endocytosis from the apical PM. At this temperature, delivery to the apical PM is blocked and both receptor-ligand complexes predominantly localize in the ARE, which is located approximately 3.5 μ m below the apical PM¹¹. Visualization of all our images and data presented takes place at this focal plane. Then, the cells are washed with PBS to remove unbound ligands and immediately fixed with 4% paraformaldehyde/PBS.

With Alexa488 acting as the donor and Cy3 as the acceptor in FRET microscopy, we internalized the Alexa488-and Cy3-labeled ligands at a D:A ratio of 1:1. In all, three different samples were used: The double-labeled specimen, containing apically internalized Alexa488-pIgA-R-ligand complexes and basolaterally internalized Cy3-pIgA-R-ligand complexes, plus corresponding single-label reference samples containing either Alexa488 or Cy3, which were used to establish the background level.

2.3 Laser Scanning 1-P and 2-P FRET Microscopy

For the 1-P data collection, we used a Nikon PCM 2000 laser scanning confocal microscope, equipped with a 60x water immersion lens 1.2 NA, Argon (488nm) and Green HeNe (543nm) laser, emission filters 515/50nm and 590nm LP for our standard experiments, respectively (Figure 2-A). For the experiments comparing different emission filters, we have used 580/20, 580/30, 580/40, 580/50, 610/75, kindly provided by Dr. C. M. Stanley (Chroma Corp. Brattleboro, VT) and our standard 590LP (Fig. 1). SimplePCI software (Compix, Cranberry Township, PA) was used to drive the hardware, image acquisition and processing. Bleaching is undetectable when the argon laser is only used for one scan to collect the final image - see below. PCM is set to collect data simultaneously in both channels at a 1024x1024 pixel image.

For the 2P-FRET experiments we used a VERDI pumped turntable mounted titanium:sapphire laser, coupled to the laser port of a Biorad MRC600 (Biorad, Hercules, CA). The MRC600 scan head is coupled to a Nikon TE300 (Eclipse) epifluorescent microscope (Nikon, Melville, NY), linked to a personal computer and monitor³ (Figure 2-B). For data collection, the same specimens were used as in the laser scanning confocal experiment. The objective was a 60x water immersion lens 1.2 NA, the laser excitation wavelength at 790nm and a 4.0 power level. We have used this laser excitation wavelength to excite specifically the donor molecules. We have used a 535/50nm donor emission filter and our standard 610/60nm acceptor filter, plus, for comparative measurements the above-mentioned 580/20-30 series. Fluorescence levels are presented simultaneously on a split screen, one representing the donor channel the other the acceptor channel.

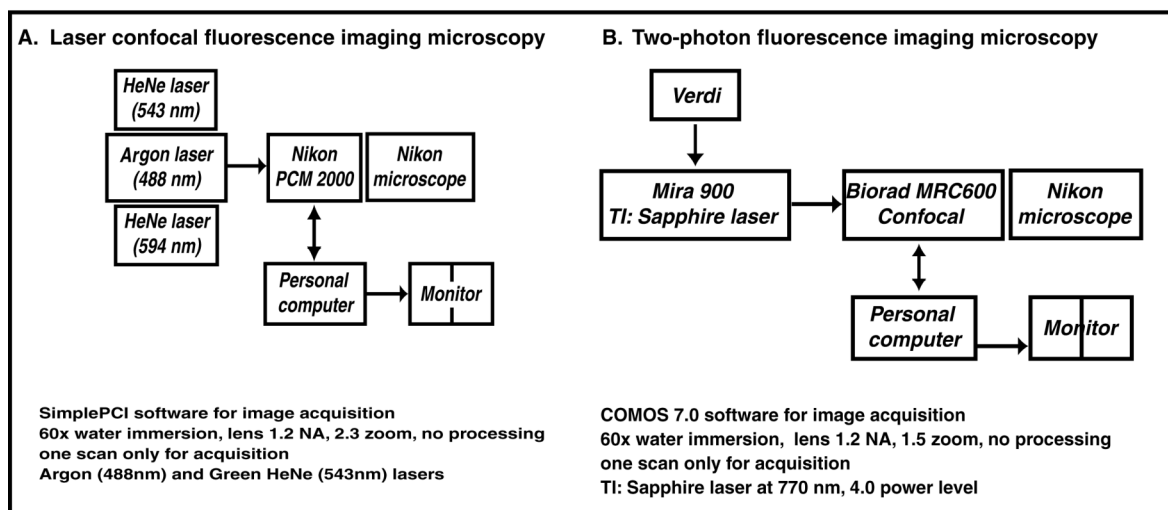


Figure 2. The two microscopy systems used in our experiments

2.4 Spectral Analysis

A specific spectral analysis of ligand-fluorophore complexes used in our experiments was performed (Fig. 1). 500 μ l of 1 μ M of [Fab]₂-Alexa 488 and [Fab]₂-Cy 3 complexes were prepared in PBS). Luminescence intensity measurements to obtain the individual spectra were carried out using a Spex Fluorolog 2+2 spectrofluorimeter. All data were collected with right angle detection at room temperature (22 \pm 2 $^{\circ}$ C) in air-saturated solutions. Excitation and emission intensity data were evaluated at the maximum.

2.5 Data Collection

For both, 1-P and 2-P microscopy, the specimen is positioned in a small chamber created by a coverslip between two metal rings and filled with a small amount of PBS. This whole assembly is placed on the microscope stage. We first select an appropriate area of the specimen, check the cell height (15-20 μ m) and a focal plane of 3.5 μ m below the apical PM, with only the Green HeNe laser in operation. With the zoom settings at 2.3 and without any image processing, a one-scan image of the double-labeled specimen is taken with only the Green HeNe laser/acceptor excitation (the argon laser is blocked). This is followed by a one-scan image with only the argon laser/donor excitation (Green HeNe laser blocked). The single-labeled acceptor specimen follows the same protocol; the single-labeled donor specimen is only scanned with the argon laser, as we do not observe fluorescence when subjected to the acceptor excitation. Images of all three types of specimen are taken under the exact same conditions: 60x water immersion lens, PCM 1024 color, 2.3 zoom, no processing.

2.6 Post-Acquisition Data Generation - Algorithm Removes Spillover Contamination

As described in the introduction, there are two contaminants in the FRET signal: donor crosstalk and acceptor bleed-through. We have developed a novel algorithm, which removes these contaminants pixel-by-pixel on the basis of matched fluorescence levels between the double-label specimen and a single-label reference specimen⁹, using seven images in all: two single-label donor reference images (donor excitation/donor channel and acceptor channel); two single-label acceptor reference images (donor and acceptor excitation, both in the acceptor channel); three double-label images (donor excitation/donor and acceptor channel, acceptor excitation/acceptor channel). For example, to remove the acceptor bleed-through, fluorescence levels are matched by pixel at the same acceptor excitation/acceptor channel conditions, between the double-label and single-label acceptor specimen. Those specific pixel location coordinates are recorded by the program and tracked to the same locations in the respective images taken at donor excitation in the acceptor channel (FRET channel). The fluorescence appearing here in the single-label specimen represents acceptor bleed-through and may be assumed to be identical in the double-label specimen at the same acceptor intensity levels, and is subsequently deducted pixel-by-pixel from the contaminated, uncorrected FRET (uFRET) signal. The donor crosstalk is removed analogously to finally achieve a corrected FRET (cFRET) image.

2.7 Post-Acquisition Data Analysis - Calculating Energy Transfer Efficiency (E%)

The calculation of E% is central to differentiating between random and clustered distribution of membrane-bound components as well as to estimate the distance between molecules^{1,10}. We have not considered the calculation of distance in our colocalization scenario, which by definition deals with variable distances. There are different ways to calculate E%^{1,10}, the principle, however, is to establish the difference between the quenched and unquenched donor fluorescence (= energy transfer) and relate that value to the unquenched donor, which expresses as a percentage of how much of the potential energy was transferred. With our algorithm-based method, cFRET represents the actual energy transfer, which we add to the quenched donor fluorescence, pixel-by-pixel, producing an unquenched donor value. This, together with the other double-label data, allows us to calculate E% ($= 100 \times \text{cFRET} / \text{quenched donor} + \text{cFRET}$) and its relationship to acceptor, donor and D:A ratios. A custom-written analysis program includes some refinements: we first select pixels between 10 and 254 arbitrary units in the uFRET image. Eliminating values below 10 arbitrary units removes background noise, which we previously established to be on average 8 arbitrary units for unlabeled cells (data not shown). By not considering pixels at 255 units (the maximum of the range) we eliminate saturated pixels. The selected uFRET pixel locations are transferred to the quenched donor image (donor excitation/donor channel) and pixels containing saturated donor fluorescence are eliminated (this is a precaution to avoid a potentially misleading calculation of the unquenched donor value; in actuality, there are very few saturated donor pixels). This final pixel selection becomes the template for all calculations. We have established that the detector spectral sensitivity is small and have considered it to be a constant along with the quantum yield and have therefore assumed that it would not affect our E% calculations.

3. RESULTS

3.1 A Model to Differentiate Between Random and Clustered Distribution

Specific molecules contained in cellular membranes can either be assembled in clusters, distributed randomly or possibly exhibit a continuum between these two states. Knowing the nature of molecular distribution may allow us to deduce sorting processes, endosomal organization and provide a platform for investigating other membrane component associations. FRET — and in particular, energy transfer efficiency - is a most suitable method to explore such molecular associations, as the molecules have to be in close proximity for FRET to occur. The relationship of E% to acceptor fluorescence is a key indicator for random vs. clustered distribution, clearly described by Kenworthy and Edidin¹⁰. Randomly distributed donors and acceptors increase their E% with increasing acceptor fluorescence, as the probability of an acceptor colocalizing with a potential donor for energy transfer, increases. Conversely, in a clustered scenario where molecules by definition are in proximity, E% is largely independent of higher acceptor levels, as in a cluster with a choice of several acceptors at FRET distance, a donor can only transfer energy to one acceptor at a time. In a clustered distribution, the donor has the greatest impact on E%, as rising levels of donor fluorescence lead to a phenomenon, i.e. the reduction of E% with increasing donor levels and the associated D:A ratios, which has not been previously described and which we regard to be a second indicator for clustering. We believe that our model accounts for this phenomenon.

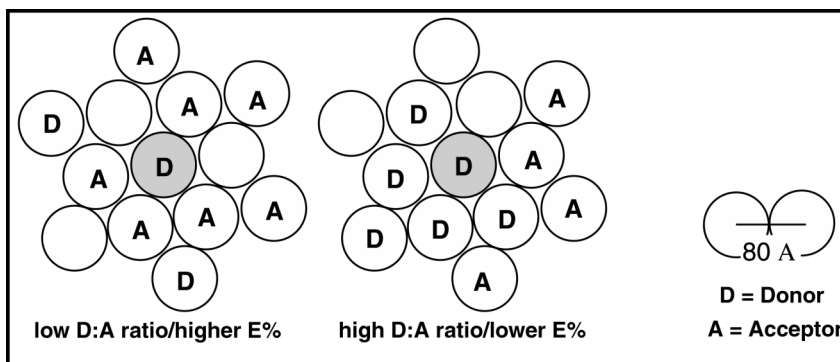


Figure 3. Two examples of different configurations of donor (D), acceptor (A) and vacant disks (empty) around a reference donor (shaded).

Our cluster model takes a number of parameters into consideration: a Förster distance of our specific donor/acceptor pair, $R_0=67.5$, an estimated diameter $R=80$ of the cylindrical space occupied by our pseudo-ligands, and 5 binding sites per pseudo-ligand for the fluorophores to attach; given the deliberately high concentration of pseudo-ligands ($160\mu\text{g/ml}$) used in our experiments, we expect all sites to be occupied by fluorophores. In our geometric model, we visualize the proteins of interest in the context of a two-dimensional surface, as disks in a plane directly above the membrane (Fig. 3). Each disk represents one molecule and in a perfectly clustered scenario, a reference donor could be surrounded by 6 other molecules, which can either be donors, acceptors, vacant (possibly other unlabeled membrane components) or a variety of combinations. As the level of donor fluorescence increases, the likelihood of a donor being adjacent to the reference donor increases, thereby preventing potential energy transfer to an acceptor, resulting in a decrease of $E\%$. We call this phenomenon donor geometric exclusion. We can also not exclude other donor-donor interaction, even though any energy transfer would not be recorded in the FRET channel. Equally, to evaluate donor competition for an acceptor would be difficult although we assume that this eventuality would run concurrently with 'donor geometric exclusion'. Figure 4A presents a simplified schematic, illustrating the effect of an increasing D:A ratio at two different levels of absolute fluorescence. Both scenarios show a reduction in $E\%$ with increasing D:A ratios, exacerbated by the increase of total absolute donor fluorescence. Our actual experimental findings in Figure 4B match this model.

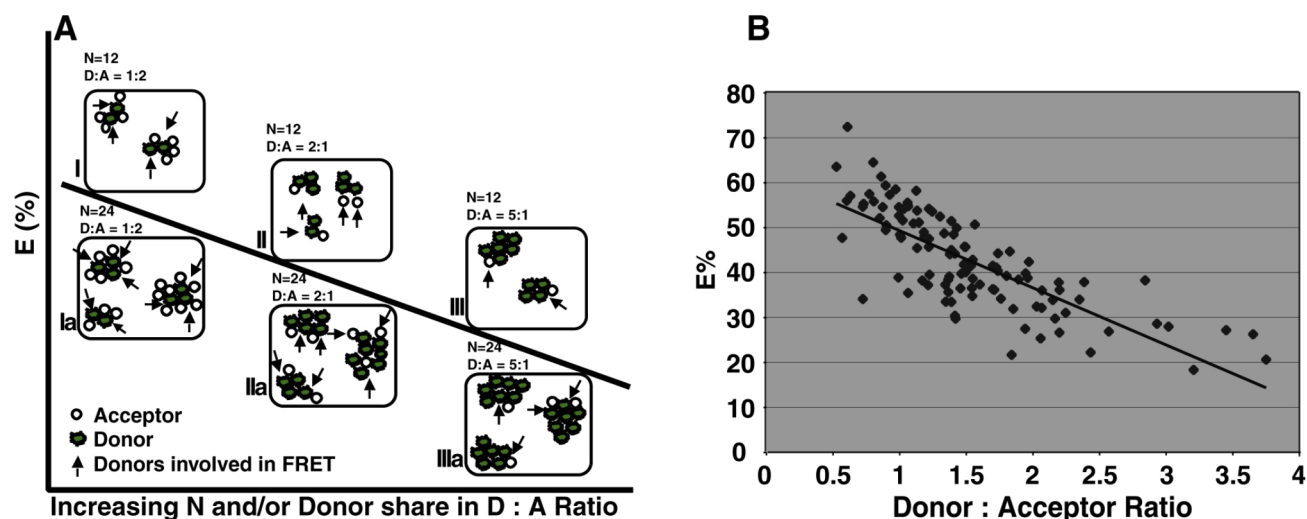


Figure 4. By definition, molecules in a cluster are in proximity. As energy arises from the donor, the donor drives $E\%$, which is largely independent of the Acceptor (Kenworthy and Edidin, 1998¹⁰). However, as donor values increase, a phenomenon occurs: 'Geometric exclusion', where donors block other donors transferring energy to an acceptor, reducing $E\%$. Both, increase in D:A ratio and absolute donor values result in a reduction. While donor-donor energy transfer does not appear in the FRET channel, it may impact the $E\%$ calculation. The experimental results closely match the model. We are proposing that the phenomenon of donor geometric exclusion is another parameter to establish a clustered distribution.

3.2 Comparing 1-P and 2-P microscopy - The Effect of Increasing Donor Fluorescence on $E\%$

When relating donor fluorescence to $E\%$, both, 1-P and 2-P microscopy results on the same specimens showed the same trends explained in our model: with increasing donor values, energy efficiency transfer markedly decreases (Figures 5A & B). 1-P microscopy extends to a somewhat higher absolute donor fluorescence compared with 2-P, and 2-P generally spreads in to lower $E\%$ ranges. Considering the different working principle between the two imaging systems, different PMT levels and spectral sensitivity, some differences are to be expected, while exhibiting a strong correlation in overall results. When we evaluate donor fluorescence by different cohorts based on levels of $E\%$, statistically different groups are evident (data not shown). The biological significance of these different cohorts still needs to be explored further; we may be looking at a continuum of sorting at steady-state, when these images of fixed cells are taken, or possibly an additional endosome apart from the ARE.

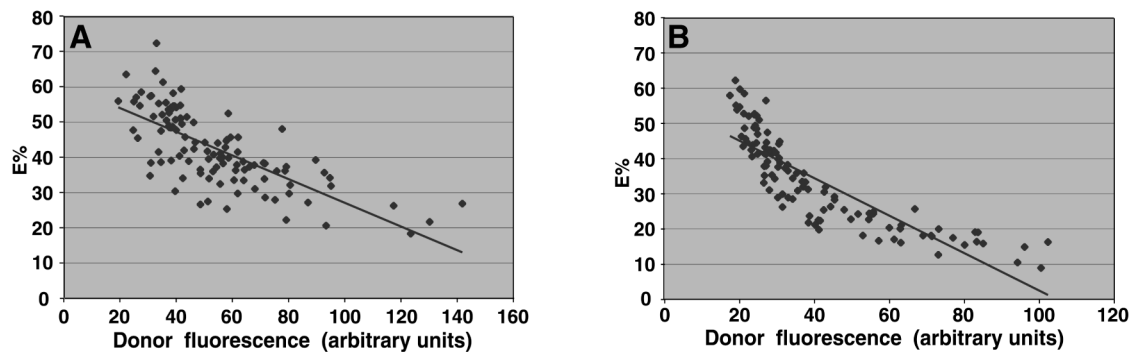


Figure 5. (A): One-photon confocal microscopy; (B): Two-photon microscopy. Colocalization of pIgA-R-ligand complexes after 4hrs of internalization from apical and basolateral PM at ARE focal plane: Energy transfer efficiency (E%) decreases with increasing donor intensity, confirming a clustered distribution, but also posing a phenomenon, explained by our model (Figure 4).

DISCUSSION AND CONCLUSION

Our experimental conditions involve a single layer of polarized epithelial MDCK cells, 15-20 μm tall, imaged at a focal plane 3.5 μm below the apical plasma membrane at a level where the apical recycling endosome (ARE) is situated. For these intracellular conditions, both the 1-P and 2-P microscopy is suitable for FRET measurements and the subsequent calculation of energy transfer efficiency (E%).

The key element for establishing a reliable level of E%, is the correct removal of contaminants of the FRET signal. Different correction methods exist which may be entirely suitable for different experimental conditions. Our novel algorithm is to be recommended for a highly sensitive method, which corrects the spillover pixel-by-pixel. Using different FRET channel emission filters allows the researcher to collect different ranges of FRET signals, albeit with different levels of contamination. We postulated that our algorithm-based correction method should compensate for the different levels of contamination by correcting FRET signal at different percentage levels while producing comparable energy efficiency transfer results. The results obtained in this paper are based on using different emission filters and our experimental findings confirmed this assumption and the robustness of the algorithm (data not shown).

We used an assay, which measures the colocalization of two differently labeled, membrane-bound complexes in the ARE. We suggest that this assay is suitable to investigate other colocalization scenarios, such as different membrane components (lipids, cholesterol), cytoskeleton related effector proteins and other proteins (e.g. Rabs) as to their association or otherwise.

We presented a clustered distribution model which explains our experimental findings of decreasing E% with increasing levels of donor fluorescence, as demonstrated in higher D:A ratios. We are suggesting that this phenomenon, not reported before, is an indicator for clustered distribution. The other, previously described determinant for this type of distribution is the independence of E% of acceptor fluorescence levels, also confirmed by our results.

Differences in E% for different regions of interest (ROI) may indicate a continuum of sorting into clusters at steady-state. We are hypothesizing that this clustering process is part of the formation of transient membrane microdomains in the ARE, prior to the establishment of vesicles, which eventually will pinch-off and proceed to the apical plasma membrane. The process of forming microdomains probably includes coat-proteins, the cytoskeleton, lipid-selfassembly, and other effectors¹³⁻¹⁶.

In summary, we conclude that the combination of the assay presented in this paper with confocal microscopy, either 1-P or 2-P, and the calculation of E% based on a novel and sensitive FRET-contamination correction algorithm, provides a reliable new method to investigate different membrane clusters/microdomain formations. We have also presented a clustered distribution model, which demonstrates a new quantitative method to measure the formation of clusters, indicated by the decrease of E% with rising donor fluorescence.

ACKNOWLEDGEMENTS

We thank Heather M. Rowe and Dr. J.N. Demas (Department of Chemistry) for their help in providing the specific luminescence spectra for Cy3 and Alexa488 conjugates. We thank Dr. C.M. Stanley of Chroma Technologies, Brattleboro, VT, for providing the different emission filter sets. We thank Sarah Smith for her assistance with the experiments and data analysis. We thank Dr. James Casanova (Department of Cell Biology, University of Virginia Medical School) for his helpful comments. We would also like to thank the members of the Keck Center for Cellular Imaging, Dr. Lance Davidson (Department of Biology, University of Virginia) as well as members of the laboratories of Dr. Barroso and Dr. Bloom (Department of Biology, University of Virginia) for helpful discussions. We would like to thank Jeff Larson from Nikon for his help with confocal microscopy.

REFERENCES

1. Lakowicz, J.R. 1999. *Principles of fluorescence spectroscopy*, second edition, Kluwer Academic/Plenum Publishers, New York.
2. Periasamy, A., Multi-photon excitation fluorescence imaging microscopy in the biomedical sciences, *SPIE*, **3604**, pp.74--82, 1999.
3. Periasamy, A., Two-photon excitation energy transfer microscopy, *SPIE*, **3921**, pp. 299-304, 2000.
4. Gordon, G.W., G. Berry, X.H. Liang, B. Levine, and B. Herman. 1998. Quantitative fluorescence resonance energy transfer measurements using fluorescence microscopy. *Biophys J.* **74**:2702-2713.
5. Bastiaens, P.I., and T.M. Jovin. 1996. Microspectroscopic imaging tracks the intracellular processing of a signal transduction protein: fluorescent-labeled protein kinase C beta I. *Proc Natl Acad Sci U S A.* **93**:8407-8412.
6. Wouters, F.S., P.I. Bastiaens, K.W. Wirtz, and T.M. Jovin. 1998. FRET microscopy demonstrates molecular association of non-specific lipid transfer protein (nsL-TP) with fatty acid oxidation enzymes in peroxisomes. *Embo J.* **17**:7179-7189.
7. Chamberlain, C., and K.M. Hahn. 2000. Watching proteins in the wild: fluorescence methods to study protein dynamics in living cells. *Traffic.* **1**:755-762.
8. Chamberlain, C.E., V.S. Kraynov, and K.M. Hahn. 2000. Imaging spatiotemporal dynamics of Rac activation in vivo with FLAIR. *Methods Enzymol.* **325**:389-400.
9. Elangovan, M., H. Wallrabe, R.N. Day, M. Barroso and A. Periasamy. 2001. Characterization of one- and two-photon fluorescence resonance energy transfer (in preparation).
10. Kenworthy, A.K., and M. Edidin. 1998. Distribution of a glycosylphosphatidylinositol-anchored protein at the apical surface of MDCK cells examined at a resolution of 100 Å using imaging fluorescence resonance energy transfer. *J Cell Biol.* **142**:69-84
11. Barroso, M., and E.S. Sztul. 1994. Basolateral to apical transcytosis in polarized cells is indirect and involves BFA and trimeric G protein sensitive passage through the apical endosome. *J Cell Biol.* **124**:83-100.
12. Brown, P.S., E. Wang, B. Aroeti, S.J. Chapin, K.E. Mostov, and K.W. Dunn. 2000. Definition of distinct compartments in polarized Madin-Darby canine kidney (MDCK) cells for membrane-volume sorting, polarized sorting and apical recycling. *Traffic.* **1**:124-140.

13. Hansen, G.H., L.L. Niels-Christiansen, L. Immerdal, W. Hunziker, A.J. Kenny, and E.M. Danielsen. 1999. Transcytosis of immunoglobulin A in the mouse enterocyte occurs through glycolipid raft- and rab17-containing compartments . *Gastroenterology*. **116**:610-622.
14. Kobayashi, T., A. Yamaji-Hasegawa, and E. Kiyokawa. 2001. Lipid domains in the endocytic pathway . *Semin Cell Dev Biol*. **12**:173-182.
15. Mukherjee, S., and F.R. Maxfield. 2000. Role of membrane organization and membrane domains in endocytic lipid trafficking . *Traffic* . **1**:203-211.
16. Woodman, P.G. 2000. Biogenesis of the sorting endosome: the role of Rab5 . *Traffic*. **1**:695-701.